06

Formation of SmS nanostructures in anodized aluminum oxide matrix

© E.B. Baskakov, S.I. Supelnyak, D.N. Khmelenin

National Research Center „Kurchatov Institute“,
123182 Moscow, Russia
e-mail: baskakov.ras@gmail.com

Received May 30, 2024
Revised July 22, 2024
Accepted August 6, 2024

The matrices made of anodized aluminum oxide with a pore diameter of 40−140 nm and 60−210 nm are made by anodizing aluminum using a two-stage method. The distribution of oxide cells and pores of matrices by diameter is presented. It was found that an increase in the etching time led to an increase in the statistical maximum of the average pore diameter from 108 to 155 nm. It was found that an increase in the pore diameter during etching is accompanied by a preservation of the size of the oxide cells and a decrease in the average thickness of the cell walls. Sic nanostructures formed in the pores of the matrices and extending to an average depth of 120 nm were obtained by magnetron sputtering. It is assumed that a conductive channel is formed in the form of a thin SmS layer connecting SmS nanostructures and a barrier layer of anodized aluminum oxide. The resistance of SmS nanostructures in a matrix of anodized aluminum oxide with Ni metallization was measured, which amounted to 23 and 22 Ω.

Keywords: anodized aluminum oxide, samarium sulfide, magnetron sputtering, nanostructures.

DOI: 10.61011/TP.2024.10.59360.196-24

Introduction

Electrochemical anodizing of pure aluminum enables the growth of highly ordered porous structures of anodized aluminum oxide (AAO). The growth mechanisms, the influence of growth process parameters on the AAO morphology [1–3], the mechanical properties [4] of porous AAO, and its structure [5,6] have already been examined in detail by several research groups. A significant number of AAO studies are focused on controlled synthesis of ordered pores relying on two principles: preliminary structuring of the initial substrate [7,8], which leads to high pore ordering, and the widely used two-stage anodizing technique [9,10], which also evolves actively in the direction of additional stimulation of self-ordering mechanisms [11–13]. The interest in controlling the configuration of AAO pores stems from their potential use as a matrix for fabrication of ordered structures, such as nanodots, nanowires, nanotubes, and membranes [14–16], with their properties differing from those of bulk or thin-film materials [17–19]. Specifically, the thermal conductivity, electrical conductivity, and thermoelectric Q-factor of one- and two-dimensional nanostructures depend on their characteristic dimensions [20–23]. Matrices based on porous AAO have the advantage of ease of fabrication of ordered porous structures over other matrices produced by lithography, molecular beam epitaxy, gas-phase deposition, and track etching of polymer membranes [3]. Thus, the design of structures with AAO matrices opens the way both to the qualitative modification of properties of the materials used and to the development of novel devices.

The specifics of deposition of samarium sulfide (SmS) into AAO pores performed with the purpose of nanostructure fabrication are discussed in the present study. SmS is known for its isostructural semiconductor−metal phase transition [24], the generation of thermal emf without an induced temperature gradient (thermovoltaic effect) [25], and other properties with practical application potential [26]. Earlier studies into the nanostructuring of bulk SmS revealed that high-temperature annealing leads to an increase in crystallite size and a reduction in the number of defective Sm ions at grain boundaries and the conductivity activation energy [27]. The most significant lowering of intergranular potential barriers is observed at 2300°C, which makes the discussed method fairly energy-intensive.

It is known that intergranular potential barriers in thin films with their thickness comparable to the grain size have a more significant effect on conductivity along the film than across it [28]. It is assumed that SmS nanostructuring with the use of an AAO matrix will enable the fabrication of columnar structures allowing for longitudinal passage of carriers without any significant reduction in mobility and scattering at potential intergranular barriers. Ordered SmS-based nanostructures may find application in thermoelectric generators, oxygen sensors, and strain gauges.

1. Materials and methods

An AAO matrix was produced by a two-stage anodizing method with reference to literature data [29,30]. The initial substrates were four disks with a thickness of 80 μm and a diameter of 19 mm cut from technical aluminum foil (Al> 99.5%, major impurities: Fe and Si< 0.5%), which were annealed for 2 h in air at 500°C in a SNOL 6/12-V muffle furnace. Annealing was performed for the

purpose of recrystallization and homogenization of the grain composition. The surface of these disks was cleaned with isopropyl alcohol and rinsed with distilled water. Two disks were kept as control samples, and the other two (samples of the 1st and 2nd series) were anodized.

The first anodizing of the samples of the 1st and 2nd series was performed using a 0.5 N solution of $(COOH)_2$ at 85 V for 30 min at a temperature of 7–13°C. Aluminum oxide was etched in an aqueous solution containing 1.8 g CrO_3 and 7.1 g 85% H_3PO_4 per 100 m*l* at 85°C for $\sim$ 10 min. The second anodizing of the samples of the 1st and 2nd series was similar to the first one, but its duration was reduced to 25 min. The produced second layer of aluminum oxide was etched under the conditions similar to those specified above for 30 s (samples of the 1st series) and 90 s (samples of the 2nd series). The obtained substrates were rinsed with distilled water.

AAO pores (Fig. 1, *a*) were filled by magnetron sputtering, which is used to obtain thin SmS films [31,32] and in the process of fabrication of structures based on AAO matrices [33–35]. The sputtering of SmS and Ni for the samples of the 1st and 2nd series (Figs. 1, *b, c*) and for the control samples (Fig. 1, *d*) was performed sequentially at a VUP-5 vacuum coater at a pressure of $5 \cdot 10^{-3}$ Pa in argon. The duration of SmS sputtering was 10 min at a power of 88 W and 30 min at 72 W for the 1st and 2nd series with control samples, respectively. The deposition of Ni metallization onto all samples was performed at a power of 114 W for 7 min. The substrate temperature was maintained at 250°C in each case. Stencil masks were used in each sputtering procedure in such a way that the SmS layer was deposited onto the AAO matrix surface, while Ni was deposited onto the SmS film surface and prevented from reaching the end faces of the AAO matrix.

The porous AAO layer surface and cleaved surfaces and transverse sections of the fabricated structures were imaged by scanning electron microscopy (SEM) with a Scios FEI field-emission scanning electron-ion microscope.

X-ray microanalysis with mapping of the distribution of elements within transverse structure sections was carried out by energy-dispersive X-ray spectroscopy using an EDAX Octane Elect Super attachment to the Scios FEI microscope. The sections for this analysis were prepared with an argon beam and a Hitachi IM4000 Plus ion milling system.

The DLgram cloud service based on deep learning technologies [38] was used to perform digital processing of SEM images of AAO pores for the purpose of quantitative analysis [11,36,37].

A laboratory setup featuring a Tektronix DMM4040 multimeter and an insulating stage was used for electrical resistance measurements. The measurement error did not exceed 1%.

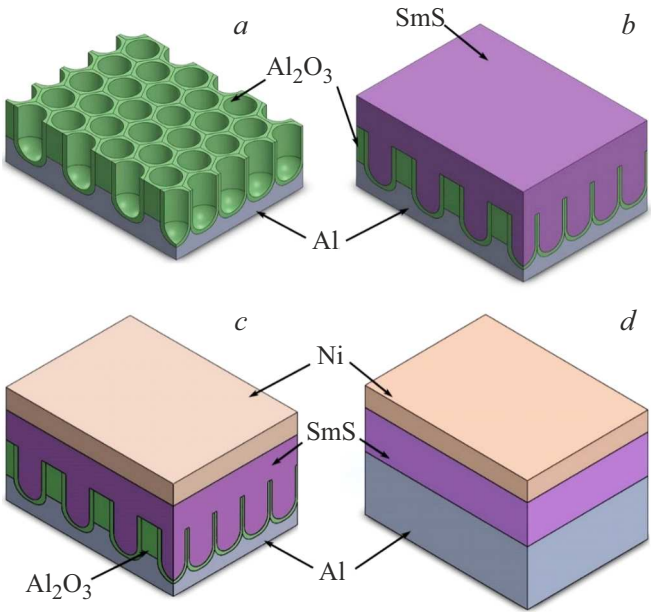

Figure 1. Schematic diagram of the fabrication of samples of the 1st and 2nd series (*a–c*) and the control sample (*d*). *a* — Formation of an anodized layer on an Al substrate; *b* — magnetron sputtering of SmS into the pores of the anodized layer; *c* — magnetron sputtering of Ni metallization; *d* — magnetron sputtering of SmS and Ni onto the Al substrate.

2. Results and discussion

Figure 2 presents typical SEM images of nanoporous AAO that reveal the formation of cylindrical pores with a diameter of 40–140 nm (1st series) and 60–210 nm (2nd series) oriented perpendicular to the surface of the aluminum substrate.

The observed differences in thickness of porous AAO between the samples of the 1st and 2nd series (Figs. 2, *b, d*) are attributable to an uneven rate of oxide growth on the Al surface in the course of the electrochemical reaction.

The DLgram service for recognition of similar objects was used to calculate the area of specific types of objects and perform quantitative and statistical analysis of the surface morphology of the obtained AAO samples. Figure 3 presents an example of recognition of objects of the AAO matrix in the sample of the 1st series.

The size of pores and cells was determined with account for their irregular shape by calculating the projection diameter, which is the diameter of a circle equal in area to the projection of a pore or cell [39]:

$$D_{pr} = (4 \cdot S_{pr}/\pi)^{1/2}.$$

The average values of area S_{pr} and projection diameter D_{pr} were estimated as an arithmetic mean of the areas and diameters of oxide cells and pores in the examined area.

The results of determination of the number and the size of oxide pores and cells are presented in Fig. 4. In series 2, the dominant size of pores formed in the AAO layer

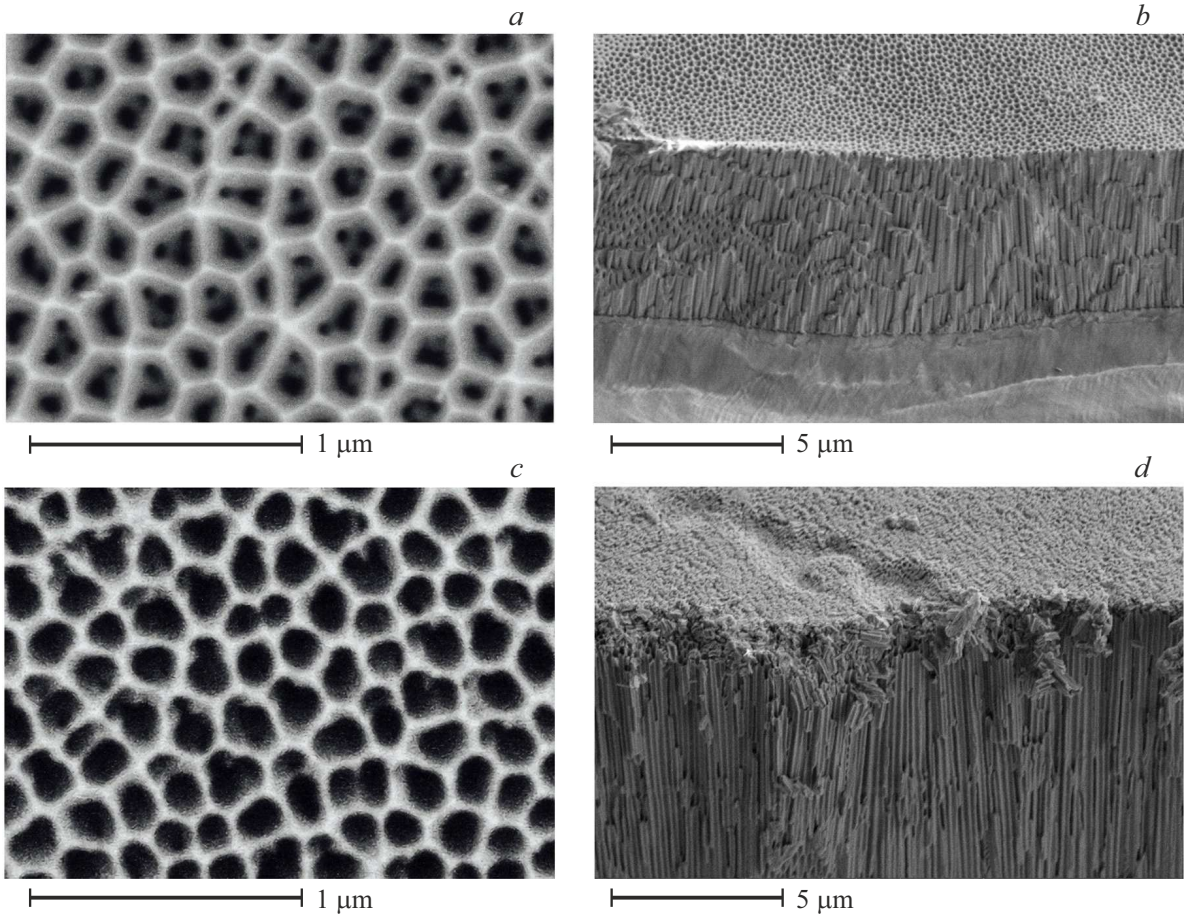

Figure 2. SEM images of the porous anodized Al_2O_3 layer. Series 1: *a* — top view; *b* — cleaved substrate; series 2: *c* — top view; *d* — cleaved substrate.

exceeds the pore diameter in series 1 by a factor of 1.4. It was found that the statistical maximum of the average pore diameter shifted from 108 to 155 nm (the 1st and 2nd series, respectively) as the etching time increased, and the etching itself also caused statistical spread of the pore diameter and contributed to the formation of a large pore instead of 2–3 smaller ones, which is especially evident in the SEM images for the 1st series (Fig. 2, *a*). Note that AAO etching in CrO_3 and H_3PO_4 leads only to an increase in pore diameter. The statistical maxima of the average diameter of oxide cells of the samples turned out to be almost identical (235 and 230 nm), and the concentrations of cells and pores in both series were $26\,\mu m^{-2}$, which is probably indicative of stability of the used AAO synthesis method. While pores grew in the course of etching, oxide cells retained their size, and the average thickness of the cell walls decreased from approximately 60 to 30 nm (the 1st and 2nd series, respectively).

It is known that the pore size and the degree of ordering of hexagonal cells in a porous AAO layer depend on the ordered structure of the aluminum surface formed in the first anodizing process [40]. It was demonstrated that the structure depends on the concentration of ions in the electrolyte, the electrophysical characteristics of the substrate, and the temperature of the substrate–electrolyte system [41,42]. The asymmetric nature of the distribution of cell sizes (Fig. 4, *b*) and the stochastic arrangement of pores (Fig. 2) are governed by the nature of mass transfer in the solution in the process of aluminum anodizing and the kinetics of diffusion of reagents in channels of the oxide film. The anodizing voltage in the electrolytic cell [42] was the parameter specifying the nature of mass transfer.

Figure 5 shows the section of the structure characteristic of samples of both series with deposited SmS and Ni layers. The Pt layer was used as a protective mask to prepare the section.

The average size of oxide cells determined from Fig. 5 (210 nm) agrees closely with the quantitative analysis data. The image of the section of the 1st series (Fig. 5, *b*) reveals etching and filling of pores with samarium sulfide to an average depth of 120 nm (with a spread from 60 to 180 nm) and a smooth transition of the average diameter from 90 to 70 nm.

The distribution maps of S (Fig. 6, *b*) and Sm (Fig. 6, *c*) plotted for the AAO section (Fig. 6, *a*) for series 2 do not correspond exactly to the AAO structure profile, which

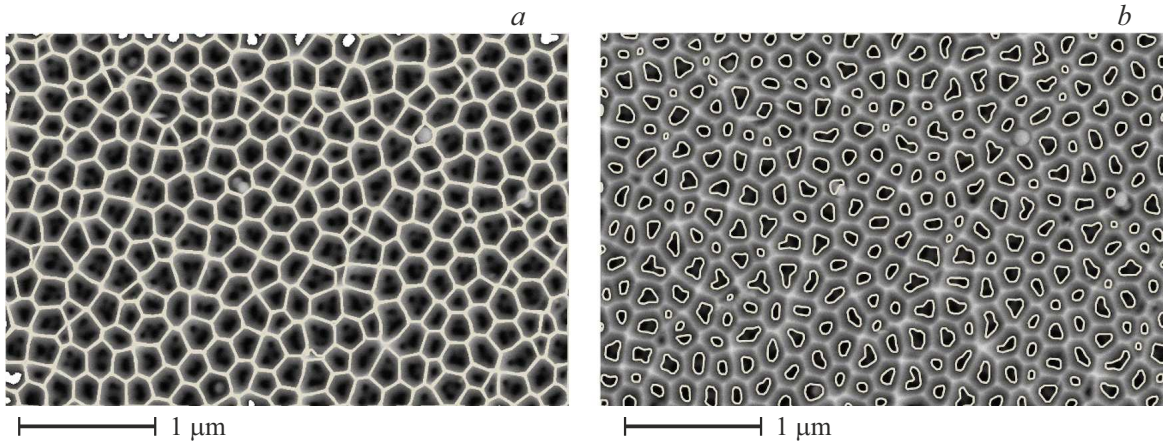

Figure 3. SEM images with highlighted objects for AAO of the 1st series: *a* — oxide cells are highlighted; *b* — pores are highlighted.

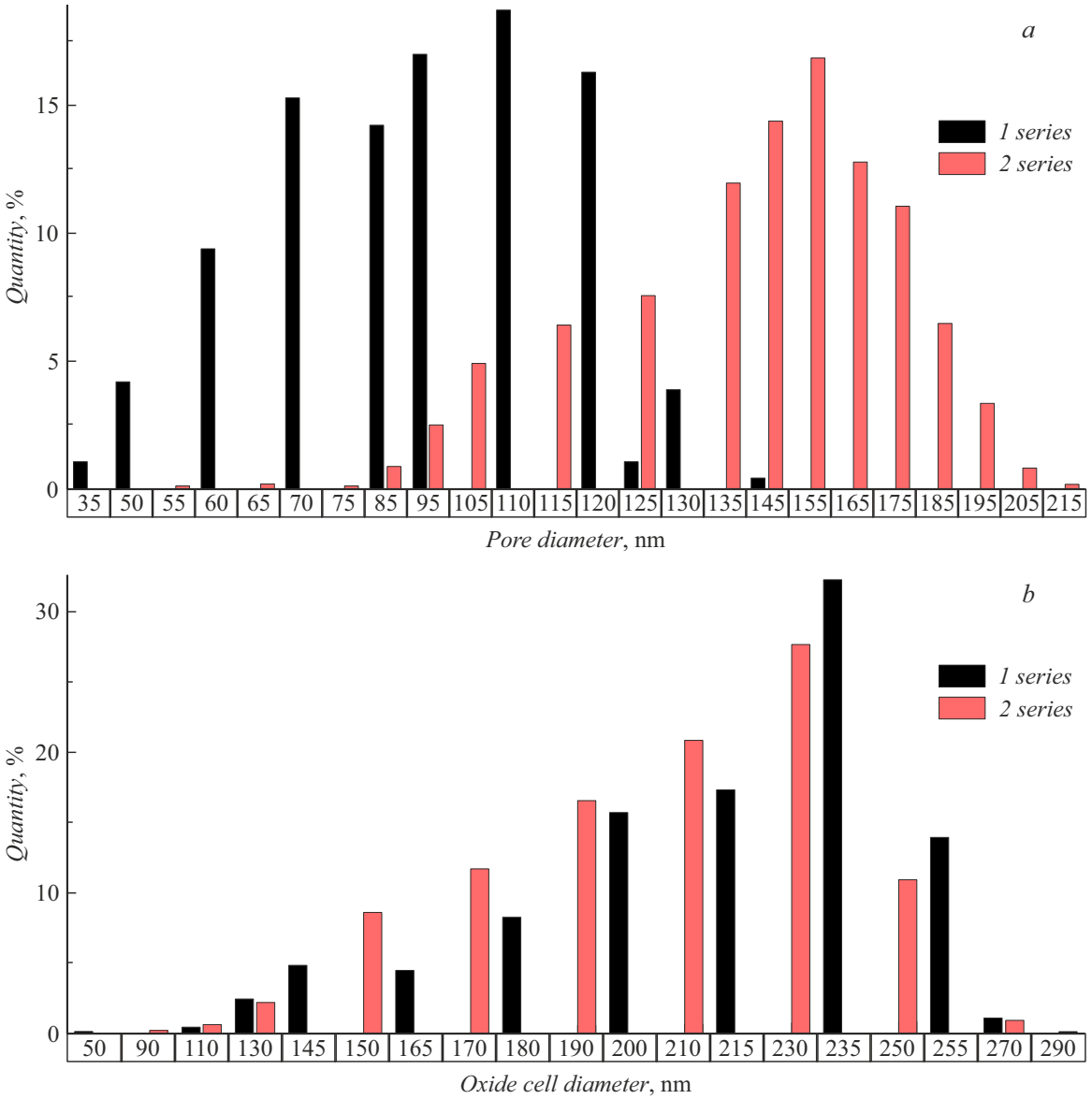

Figure 4. Diagrams of size distributions of AAO pores (*a*) and cells (*b*).

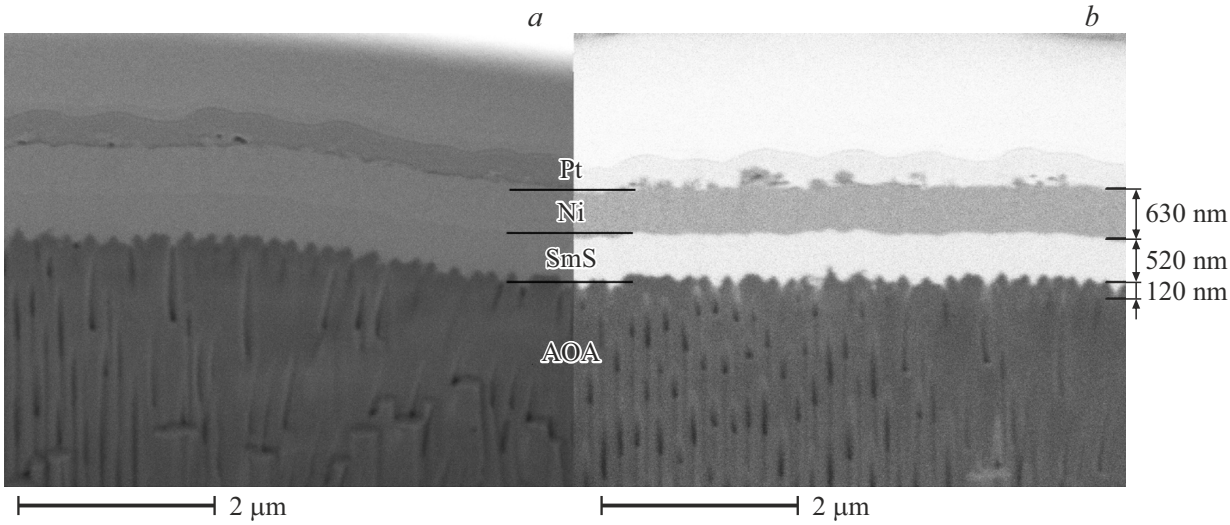

Figure 5. SEM images of the $Al_2O_3-SmS-Ni$ structure section of the sample of the 1st series. Imaging was performed in the modes of detection of secondary electrons (*a*) and backscattered electrons (*b*).

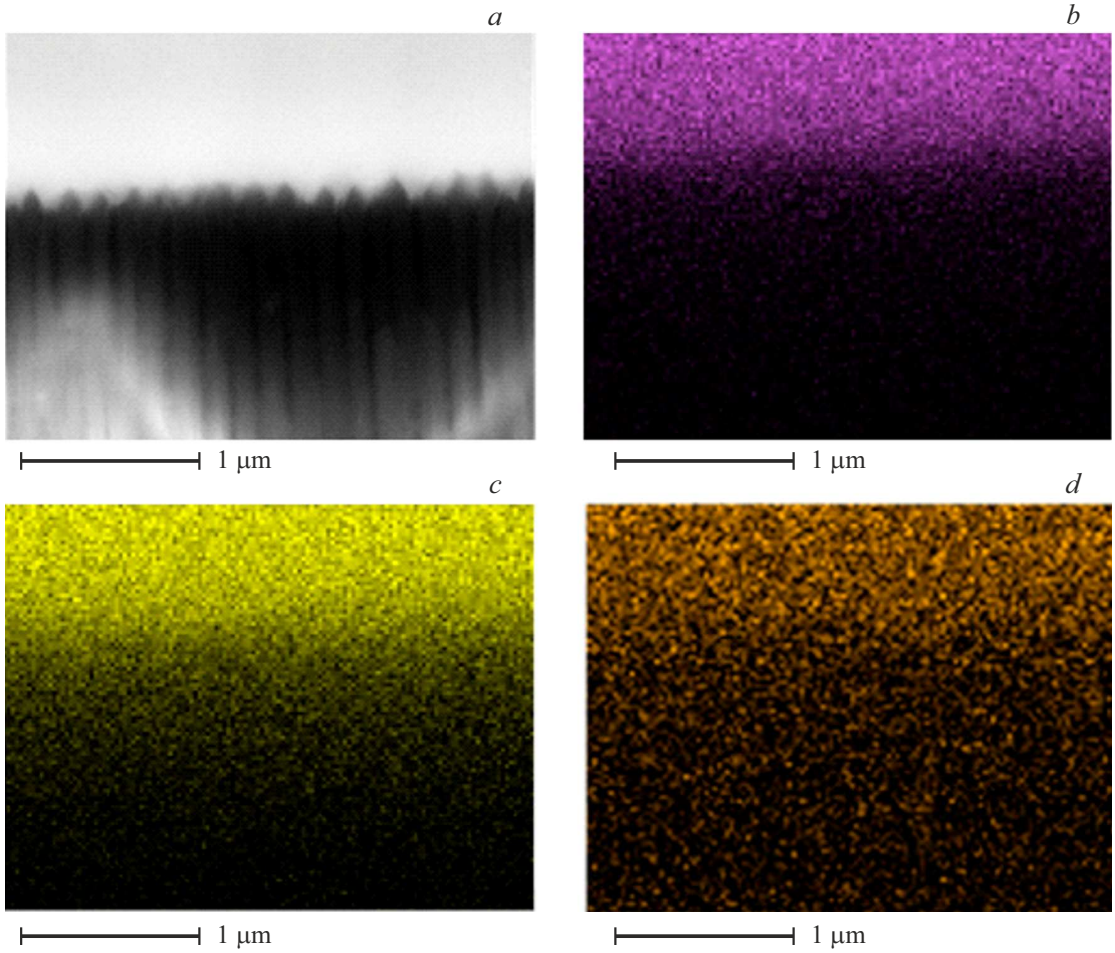

Figure 6. Images of a fragment of the $Al_2O_3-SmS-Ni$ structure section of the sample of the 2nd series. *a* — SEM image; element distribution maps for it: *b* — S; *c* — Sm; *d* — Ni.

may be attributed to non-uniform condensation of materials removed during ion etching on the section surface; this is also confirmed by the distribution map of Ni that made it to the AAO section (Fig. 6, *d*). In the examined part of the

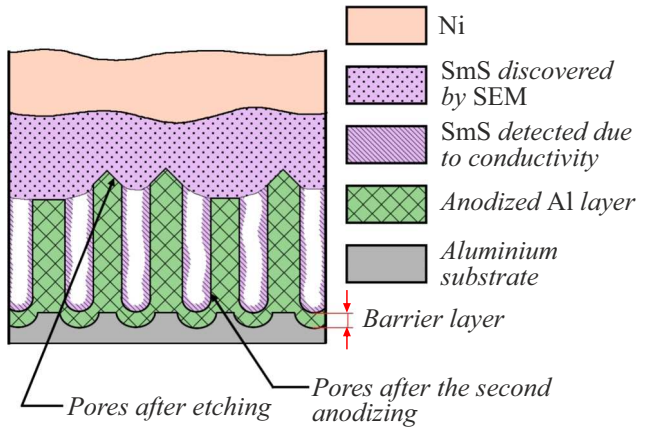

Figure 7. Schematic diagram of filling of the AAO structure with SmS.

sample, the atomic percentage ratio of Sm to S was 1 : 0.74, which indicates a deficiency of S in the film composition and is a feature of magnetron sputtering [43].

Thus, the electron microscopy data did not allow us to estimate the filling of the unetched pore part with samarium sulfide (Fig. 5). However, electrical conductivity between the substrate and the upper Ni contact was detected after the deposition of the discussed structure, and the resistance for series 1 and 2 was 23 and 22 Ω, respectively. The resistances of the control samples were 1 Ω with an SmS deposition time of 10 min and 9 Ω at a deposition time of 30 min. It is known that AAO is a dielectric with a specific resistance of $4 \cdot 10^{16}$ Ω·cm [44] and the AAO matrix is characterized by the presence of a barrier layer with a thickness of several tens of nanometers [3] (Fig. 7). Since the barrier layer is quite thin compared to the obtained AAO matrix, a comparison of the electrical resistances of samples of series 1 and 2 with the control ones suggests that a layer of SmS did actually form on the walls of pores throughout their entire depth.

Conclusion

Samarium sulfide nanostructures were formed using nanoporous AAO templates, and the shape and size of cells and pores of the oxide layer and the SmS layer were analyzed. It was demonstrated that anodizing with a 0.5 N solution of $(COOH)_2$ at 85 V yields an asymmetric distribution of cell sizes and a stochastic pore arrangement. It was found that the statistical maximum of the average pore diameter increases with an increase in etching time. It was demonstrated that the average depth of pore filling with samarium sulfide was 120 nm with a smooth variation of the average diameter from 90 to 70 nm. Electrical conductivity was observed after the deposition of the discussed structure, which suggests that a thin SmS layer did indeed form on the walls of pores throughout their entire depth.

Acknowledgments

The authors wish to thank the lead researcher of the Electron Microscopy Laboratory V.V. Artemov for SEM imaging of AAO and the lead engineer of the Crystal Growth Laboratory A.V. Bezrukov for magnetron sputtering of thin SmS and Ni films.

Funding

This study was carried out under the state assignment of National Research Center „Kurchatov Institute.“ Equipment provided by common use center „Structural Diagnostics of Materials“ (Kurchatov Complex „Crystallography and Photonics,“ National Research Center „Kurchatov Institute“) was used for electron microscopic imaging.

Conflict of interest

The authors declare that they have no conflict of interest.

References

[1] J.W. Diggle, T.C. Downie, C.W. Goulding. Chem. Rev., **69**, 385 (1969).
[2] G.E. Thompson, G.C. Wood. Treatise on Mater. Sci. Technol., **23**, 250 (1983). DOI: 10.1016/B978-0-12-633670-2.50010-3
[3] G.D. Sulka. *Highly Ordered Anodic Porous Alumina Formation by Self-Organized Anodizing.* In A.Eftekhari (ed.). *Nanostructured Materials in Electrochemistry*, Ch.1 (Wiley-VCH Verlag GmbH & Co, 2008), DOI: 10.1002/9783527621507.ch1
[4] C.E. Alvey. *The Mechanical Properties of Porous Anodic Oxide Films on Aluminium* (The University of Manchester Institute of Science and Technology, Manchester, 1974)
[5] F. Keller, M.S. Hunter, D.L. Robinson. J. Electrochem. Society, **100** (9), 411 (1953). DOI: 10.1149/1.2781142
[6] J.P. O'sullivan, G.C. Wood. Proceed. Royal Society of London. A. Mathem. Phys. Sci., **317** (1531), 511 (1970). DOI: 10.1098/rspa.1970.0129
[7] H. Masuda, H. Yamada, M. Satoh, H. Asoh, M. Nakao, T. Tamamura. Appl. Phys. Lett., **71** (19), 2770 (1997). DOI: 10.1063/1.120128
[8] S. Shingubara, Y. Murakami, K. Morimoto, T. Takahagi. Surf. Sci., **532**, 317 (2003). DOI: 10.1016/S0039-6028(03)00433-3
[9] H.M.H. Masuda, M.S.M. Satoh. Jpn. J. Appl. Phys., **35** (1B), L126 (1996). DOI: 10.1143/JJAP.35.L126
[10] X.Y. Han, W.Z. Shen. J. Electroanalytical Chem., **655** (1), 56 (2011). DOI: 10.1016/j.jelechem.2011.02.008
[11] C. Cheng, A.H.W. Ngan. Nanotechnology, **24** (21), 215602 (2013). DOI: 10.1088/0957-4484/24/21/215602
[12] A.I. Vorobyova, E.A. Outkina. Russ. Microelectron., **34** (3), 147 (2005). DOI: 10.1007/s11180-005-0023-6
[13] S. Ono, M. Saito, H. Asoh. Electrochim. Acta, **51** (5), 827 (2005). DOI: 10.1016/j.electacta.2005.05.058
[14] J. Liang, H. Chik, J. Xu. IEEE J. Selected Topics in Quant. Electron., **8** (5), 998 (2002). DOI: 10.1109/JSTQE.2002.804238

[15] V.M. Fedosyuk. Izv. Nats. Akad. Nauk Belarusi. Ser. Fiz.-Tekh. Nauk, **66** (1), 37 (2021) (in Russian). DOI: 10.29235/1561-8358-2021-66-1-37-46
[16] H. Masuda, K. Fukuda. Science, **268** (5216), 1466 (1995). DOI: 10.1126/science.268.5216.1466
[17] K.X. Wang, Z. Yu, V. Liu, M.L. Brongersma, T.F. Jaramillo, S. Fan. Acs Photonics, **1** (3), 235 (2014). DOI: 10.1021/ph4001026
[18] S. McNamee, D. Wagner, E.M. Fiordaliso, D. Novog, R.R. LaPierre. Nanotechnology, **30** (7), 075401 (2018). DOI: 10.1088/1361-6528/aaf30a
[19] K. Koshelev, S. Kruk, E. Melik-Gaykazyan, J.H. Choi, A. Bogdanov, H.G. Park, Y. Kivshar. Science, **367** (6475), 288 (2020). DOI: 10.1126/science.aaz3985
[20] L.D. Hicks, T.C. Harman, X. Sun, M.S. Dresselhaus. Phys. Rev. B, **53** (16), R10493 (1996). DOI: 10.1103/PhysRevB.53.R10493
[21] D. Li, Y. Wu, P. Kim, L. Shi, P. Yang, A. Majumdar. Appl. Phys. Lett., **83** (14), 2934 (2003). DOI: 10.1063/1.1616981
[22] A. Stranz, Ü. Sökmen, J. Kähler, A. Waag, E. Peiner. Sensors and Actuators A: Phys., **171** (1), 48 (2011). DOI: 10.1016/j.sna.2011.01.022
[23] X. Zou, X. Chen, H. Huang, Y. Xu, W. Duan. Nanoscale, **7** (19), 8776 (2015). DOI: 10.1039/c5nr01892g
[24] I.A. Smirnov, V.S. Oskotskii. Sov. Phys. Usp., **21**, 117 (1978). DOI: 10.1070/PU1978v021n02ABEH005517
[25] M.M. Kazanin, V.V. Kaminskii, S.M. Solov'ev. Tech. Phys., **45** (5), 659 (2000). DOI: 10.1134/1.1259698
[26] A. Sousanis, P.F. Smet, D. Poelman. Materials, **10** (8), 953 (2017). DOI: 10.3390/ma10080953
[27] V.V. Kaminskii, S.A. Kazakov, M.V. Romanova, N.V. Sharenkova, M.A. Grevtsev. Phys. Solid State, **57** (2), 277 (2015). DOI: 10.1134/S106378341502016X
[28] A. Fahrenbruch, R. Bube. *Fundamentals of Solar Cells. Photovoltaic Solar Energy Conversion* (Academic Press, 1983).
[29] A.Yu. Stepanova, I.V. Zaporotskova, A.N. Belov. Vestn. Volgogr. Gos. Univ., **10** (5), 114 (2011) (in Russian).
[30] D.O. Il'in. *Sintez i lyuminestsentnye svoistva nanoporistykh struktur anodirovannogo oksida alyuminiya* (Ural. Fed. Univ., Ekaterinburg, 2015) (in Russian).
[31] V.I. Strelov, E.B. Baskakov, U.N. Bendryshev, V.M. Kanevskii. Crystallography Reports, **64** (2), 311 (2019). DOI: 10.1134/S1063774519020299
[32] V.G. Bamburov, O.V. Andreev, V.V. Ivanov, A.N. Voropai, A.V. Gorshkov, A.A. Polkovnikov, A.N. Bobylev. Dokl. Phys. Chem., **473** (2), 66 (2017).
[33] Z. Fang, Y. Wang, X. Peng, X. Liu, C. Zhen. Mater. Lett., **57** (26–27), 4187 (2003). DOI: 10.1016/S0167-577X(03)00287-8
[34] N. Nuntawong, M. Horprathum, P. Eiamchai, K. Wong-Ek, V. Patthanasettakul, P. Chindaudom. Vacuum, **84** (12), 1415 (2010). DOI: 10.1016/j.vacuum.2009.12.020
[35] W. Cheng, Y. Zhou, X. Guan, Y. Hui, S. Wang, X. Miao. Mater. Manufacturing Processes, **31** (2), 173 (2016). DOI: 10.1080/10426914.2015.1019130
[36] H.T. Dinh, N.V. Lushpa, K.V. Chernyakova, I.A. Vrublevsky. Dokl. BGUIR, **4** (122), 79 (2019) (in Russian).
[37] V.A. Moshnikov, E.N. Sokolova, Yu.M. Spivak. Izv. SPbGETU LETI, **2**, 13 (2011) (in Russian).
[38] A.V. Matveev, A.V. Nartova, N.N. Sankova, A.G. Okunev. Microscopy Research and Technique, **87** (5), 991 (2024). DOI: 10.1002/jemt.24480
[39] A.V. Matveev, M.Yu. Mashukov, A.V. Nartova, A.G. Okunev. *Tezisy dokladov Vosemnadtsatoi Natsional'noi konferentsii po iskusstvennomu intellektu s mezhdunarodnym uchastiem KII-2020* (M., 2020), p. 230 (in Russian).
[40] H. Masuda, K. Fukuda. Science, **268** (5216), 1466 (1995). DOI: 10.1126/science.268.5216.1466
[41] A.I. Vorobyova, E.A. Outkina, A.A. Khodin. Russ. Microelectron., **36** (6), 384 (2007). DOI: 10.1134/S1063739707060054
[42] E.O. Gordeeva, I.V. Roslyakov, D.I. Petukhov, T.B. Shatalova, K.S. Napolskii, A.I. Sadykov, T.A. Suchkova. Russ. J. Electrochem., **54** (11), 990 (2018). DOI: 10.1134/S1023193518130165
[43] E.B. Baskakov, V.I. Strelov. Crystallography Reports, **66** (6), 1078 (2021). DOI: 10.1134/S1063774521060055
[44] N.D. Tomashov, M.N. Tyukina, F.P. Zalivalov. *Tolstosloinoe anodirovanie alyuminiya* (Mashinostroenie, M., 1966) (in Russian).

Translated by D.Safin